Triangular Kondo lattice in YbV_6Sn_6 and its quantum critical behavior in a magnetic field

Kaizhen Guo,[1] Junyao Ye,[1] Shuyue Guan,[1] and Shuang Jia[1,2,3,*]

[1]*International Center for Quantum Materials, School of Physics, Peking University, Beijing 100871, China*

[2]*Interdisciplinary Institute of Light-Element Quantum Materials and Research Center for Light-Element Advanced Materials, Peking University, Beijing 100871, China*

[3]*CAS Center for Excellence in Topological Quantum Computation, University of Chinese Academy of Sciences, Beijing 100190, China*

(Received 25 October 2022; revised 17 May 2023; accepted 18 May 2023; published 26 May 2023)

We report on the magnetization, specific heat, and electrical resistivity for a newly discovered heavy-fermion (HF) compound, YbV_6Sn_6, which is crystallized in a hexagonal $HfFe_6Ge_6$-type structure, highlighted by the stacking of the triangular ytterbium sublattice and kagome vanadium sublattice. Above 2 K, YbV_6Sn_6 shows typical HF properties due to the Kondo effect on the Kramers doublet of Yb^{3+} ions in the crystalline electric field. A remarkable magnetic ordering occurs at $T_N = 0.40$ K in zero field, while a weak external field suppresses the ordering and induces non-Fermi-liquid behavior. In strong magnetic field, the compound shows a heavy Fermi-liquid state. YbV_6Sn_6 is represented as one of the few examples of Yb-based HF compounds hosting a triangular Kondo lattice on which a magnetic field induces quantum criticality near zero temperature.

DOI: 10.1103/PhysRevB.107.205151

I. INTRODUCTION

Research on the heavy-fermion (HF) compounds has been an important part of strongly correlated physics in the past few decades [1–3]. As the relevant energy scales are small in the HF compounds, their ground states can be readily tuned, which provides convenience in the laboratory for the induction of quantum critical points (QCPs) through pressure, magnetic field, and chemical substitution [4,5]. Quantum fluctuation dominates near QCPs, in which highly collective excitation and exotic quantum phases emerge. The most striking is unconventional superconductivity near an antiferromagnetic (AFM) QCP, which has been explored in many Ce- and U-based HF compounds [6,7]. A ferromagnetic (FM) QCP was reported in stoichiometric $CeRh_6Ge_4$ [8] as well.

In a classical Doniach phase diagram, the competition between the Kondo effect and Ruderman-Kittel-Kasuya-Yosida (RKKY) interaction determines the ground state of the HF compounds [9]. While the Doniach scenario predicts a single QCP between the AFM ordering and heavy Fermi-liquid (FL) state, recent experimental studies revealed that it is insufficient for describing the various quantum critical behaviors in many HF compounds [10] because the frustration effect also plays an important role. Studies on HF compounds hosting a geometrically frustrated Kondo lattice, for example, the Ce-based distorted kagome lattice in CePdAl [11–13] and CeRhSn [14], have helped to build up a two-dimensional global diagram determined by the interplay between the Kondo effect and the strength of magnetic frustration [15–17].

Since Yb ions are more localized, or are likely to exist as nonmagnetic divalent ions, Yb-based HF compounds are relatively rare. The large vapor pressure of the Yb element makes it difficult to synthesize the compounds as well. Unconventional superconductivity and non-Fermi-liquid (NFL) behavior were observed in $YbAlB_4$ [18] and $YbRh_2Si_2$ [19]. The magnetic field can induce various quantum critical behaviors including NFL behavior and multiple phase transitions in YbPtBi [20] and YbAgGe [21]. Studies on Yb-based HF compounds have advanced the understanding of the NFL, the Fermi surface reconstruction, and the global phase diagram of HF systems [2,22].

Ytterbium-based compounds containing a geometrically frustrated lattice are particularly interesting because the effective spin of the Kramers doublet, crystalline-electric-field (CEF) ground state of the Yb^{3+} ion can be $J_{eff} = 1/2$. These compounds provide fertile ground for exploring exotic quantum states of matter such as the valence bond solid (VBS) and quantum spin liquid (QSL) caused by the frustration-enhanced zero-point motions of spins [16,23]. It was reported that the Yb-based Shastry-Sutherland lattice in Yb_2Pt_2Pb is close to an AFM QCP [24–26]. The Yb-based triangular lattices in the insulators $YbMgGaO_4$ [27] and $NaYbO_2$ [28] were found to be a platform for exploring the QSL physics. On the other hand, intermetallic compounds containing a Yb-based triangular lattice, in which both the Kondo effect and geometrical frustration play a role, have been less explored. Theoretical studies on the triangular Kondo lattice have suggested multiple quantum states, from various chiral-type magnetic orderings which may bring the spontaneous Hall effect [29,30] to the partial Kondo screening (PKS) state in which a subset of moments form a Kondo singlet [31,32]. The discovery of Yb-based HF compounds with a triangular Kondo lattice will provide an ideal playground for exploring the exotic states, while the quantum control of the states will help us to better understand the global phase diagram [33,34].

In studies on the RMn_6Sn_6 family [35,36], we noticed that the $HfFe_6Ge_6$-type structure may serve as an ideal framework

*gwljiashuang@pku.edu.cn

for bearing the Yb-based triangular Kondo lattice. The "166" structure is highlighted by a kagome lattice of transition metal atoms and a triangular lattice of rare earth atoms. The exploration of kagome materials in the "166" family has motivated wide interest in strongly correlated and topological physics. The previous focus was on the novel topological properties of the flat band and Dirac band in the kagome lattice [37–40]. Although it was unveiled that the rare earth elements play an important role in the magnetic structure and topological properties in kagome magnets [36], the $4f$ electronic strong correlation is less reported in the grand "166" family. Studies on $YbMn_6Sn_6$ and $YbMn_6Ge_6$ demonstrated the valence change and magnetic ordering of Yb ions [41–43]. There are few reports on the physical properties of other Yb-based "166" compounds [44,45].

We successfully grew single crystals of two new Yb-based "166" compounds, YbV_6Sn_6 and $YbCr_6Ge_6$, in the past two years. While a characterization for the latter will be presented in a forthcoming publication, we present the crystal structure, magnetization, specific heat, and electrical resistivity for YbV_6Sn_6 in this paper. The existence of the RV_6Sn_6 (R = Y, Gd–Tm, Lu) family was first reported by Romaka *et al.* in 2011 [46], but the physical properties of this family were not reported until very recently. In general, RV_6Sn_6 (R = Gd–Tm) exhibit the physical properties of well-defined $4f$-local-moment-bearing, weakly interacting magnetic intermetallic compounds [47–51]. Our measurements on YbV_6Sn_6 above 2 K showed typical properties of HF compounds, including a large electronic specific-heat coefficient and a broad peak in the $4f$ part of the temperature-dependent resistivity. Moreover, we found a remarkable magnetic ordering at 0.40 K in zero field. A weak magnetic field can suppress the ordering and induce NFL behavior. In a strong magnetic field, the compound enters a heavy FL state with an electronic specific-heat coefficient $\gamma > 400$ mJ mol^{-1} K^{-2}. Our study reveals YbV_6Sn_6 as a rare example of a HF compound hosting a Yb-based triangular Kondo lattice. The magnetic ordering and ground state below 0.4 K are likely nontrivial. YbV_6Sn_6 has the potential to be a model system for better understanding the global phase diagram in HF physics.

II. EXPERIMENT

Single crystals of YbV_6Sn_6 and LuV_6Sn_6 were synthesized via the self-flux method. The starting elements of Yb (pieces, 99.9%), Lu (pieces, 99.9%), V (grains, 99.9%), and Sn (shots, 99.97%) with the molar ratio $R : V : Sn = 1 : 6 : 20$ were placed in an alumina Canfield crucible set (CCS) [52], which is effective at preventing samples from contacting the silica wool, and then sealed in a vacuum silica ampoule. To avoid there being a slight reaction between Yb and the alumina crucible, the small pieces of Yb and V were placed close together and surrounded by droplets of Sn. The flux mixtures were heated to 1125 °C, allowed to dwell for 12 h, then continuously cooled at 2 °C/h, and finally centrifuged at 780 °C to remove excess flux. The yielded crystals were thin hexagonal plates with the dimensions $1 \times 1 \times 0.2$ mm^3 [inset in Fig. 1(c)]. Other RV_6Sn_6 (R = Gd–Tm) single crystals can also be grown using this method. The samples were soaked in dilute hydrochloric acid for a short time to dissolve the excess tin flux on the surface. The crystal structure was confirmed by performing powder x-ray diffraction (PXRD) measurements at room temperature using a Rigaku Mini-flux 600 instrument.

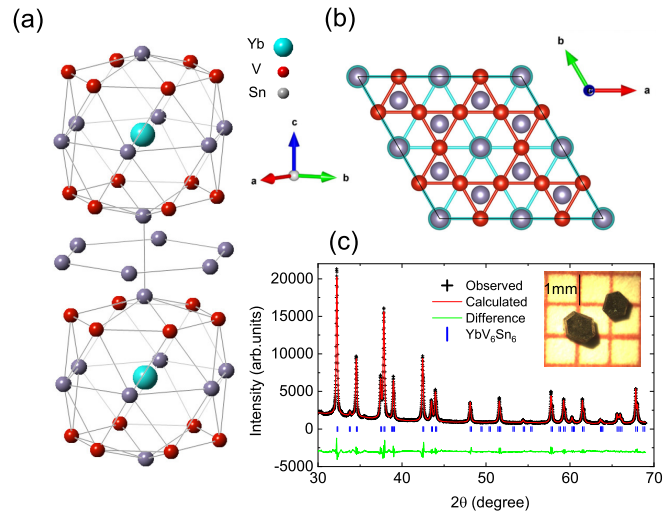

FIG. 1. (a) Crystal structure of YbV_6Sn_6. (b) Triangular and kagome lattices formed by Yb and V atoms, respectively. (c) Measured (black pluses) and calculated (red curve) powder x-ray diffraction patterns. The vertical blue bars are calculated peak positions. Inset: a photograph of single crystals of YbV_6Sn_6.

Resistance and heat capacity measurements were carried out using a Quantum Design Physical Properties Measurement System (PPMS). The resistance measurement was performed using a standard four-probe method with the current flowing perpendicular to the c axis. A dilution refrigerator (DR) unit was used to measure low-temperature resistance and heat capacity from 0.2 to 4 K. To avoid sample heating, an alternating current (ac) of $I = 0.2$ mA at a frequency of $f = 33.6$ Hz was used. Magnetization measurements were carried out using a Quantum Design Magnetic Properties Measurement System (MPMS-3) with a He-3 option. The magnetization measurement revealed that the sample contains about 0.07 vol % tin impurity, which contributed a small superconducting diamagnetic signal below 4 K in a magnetic field of less than 400 Oe. To avoid misreading the low-temperature magnetic susceptibility in weak fields, we have subtracted the diamagnetic signal of superconductive tin from the raw data.

III. RESULTS

A. Crystal structure

Most of the "166" compounds consisting of R, transition metals (T = V, Cr, Mn, Fe, Co), and germanium or tin atoms crystallize in a $P6/mmm$ $HfFe_6Ge_6$-type structure [53], including YbV_6Sn_6. Highlighted by the pristine T-based kagome and R-based triangular lattices [Fig. 1(b)], the $HfFe_6Ge_6$-type structure can be viewed as an R-stuffed CoSn-type structure, in which the R atom is caged in the polyhedron made by 12 T and 8 Sn atoms [Fig. 1(a)]. The stuffed R atom pushes the Sn sites at the top and bottom of the void space away from the hexagonal center of the V-based kagome net, leading to an alternation of stuffed and empty

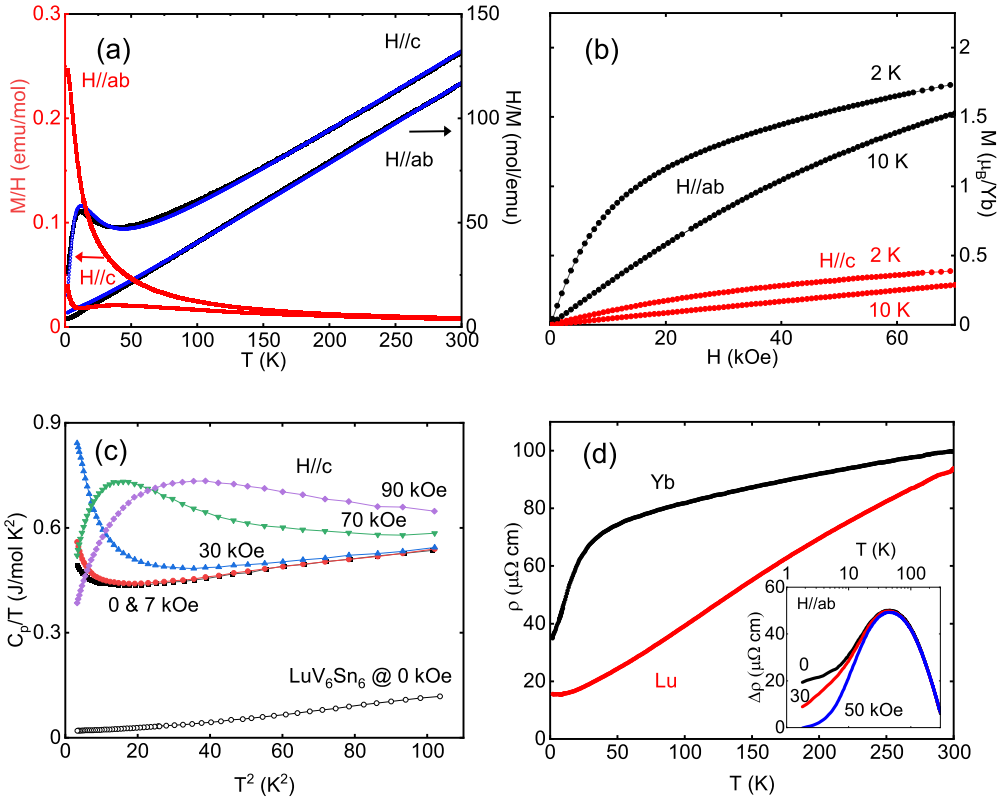

FIG. 2. Heavy fermion in YbV_6Sn_6 above 2 K. (a) The magnetic susceptibility (red curves) and its inverse (black curves) in a magnetic field of $H = 30$ kOe for $H \parallel ab$ plane and $H \parallel c$ axis. The purple curves represent the result of CEF fitting, which will be discussed later. (b) Field-dependent magnetization at 2 and 10 K. (c) Low-temperature specific heat C_p divided by temperature, as a function of T^2 in different magnetic fields along the direction of the c axis. The bottom curve represents the data for LuV_6Sn_6 for comparison. (d) Temperature-dependent resistivity of YbV_6Sn_6 and LuV_6Sn_6 in zero field. Inset: $\Delta\rho$ vs T for YbV_6Sn_6 with the resistivity of LuV_6Sn_6 subtracted, from 1.8 to 100 K, with the applied fields $H \parallel ab$ plane.

cavities along the c axis. Such an arrangement leads to an extremely large nearest Yb-Yb distance ($c = 9.1701$ Å) along the crystallographic c axis, while the nearest in-plane Yb-Yb distance of the triangular lattice is $a = 5.5020$ Å. The lattice parameters for YbV_6Sn_6 are slightly larger than those for LuV_6Sn_6 ($a = 5.5016$ Å and $c = 9.1692$ Å), indicating the presence of trivalent Yb ions at room temperature.

We compare the parameters of the Yb-based triangular lattice with those in $YbAl_3C_3$ ($a = 3.399$ Å and $c = 8.56$ Å) [54,55] and YbCuSi ($a = 3.58$ Å and $c = 4.13$ Å) [56]. In the distorted Yb kagome lattice in YbAgGe, the nearest in-plane Yb-Yb distance is 3.664 Å, while the stacking distance is 4.14 Å [57]. Apparently, YbV_6Sn_6 has the longest stacking distance and a relatively large in-plane distance. We expect a weak, anisotropic RKKY interaction between the local moments associated with the Yb^{3+} ions.

B. Heavy fermion

Temperature-dependent magnetic susceptibility $\chi(T)$ measurements were carried out on YbV_6Sn_6 in a 30 kOe applied magnetic field along the c axis ($H_{\parallel c}$) and in the ab plane ($H_{\parallel ab}$) [Fig. 2(a)]. A large easy-plane anisotropy was observed at all temperatures. When $H_{\parallel c}$ is applied, $\chi(T)$ exhibits a broad local maximum at around 45 K, followed by a slight decrease to a local minimum at approximately 12 K, and then increases again as the temperature decreases. In comparison, $\chi(T)$ for $H \parallel ab$ plane does not exhibit any anomaly down to 2 K. The anisotropic $\chi(T)$ profile of YbV_6Sn_6 is similar to that observed for Yb_2Pt_2Pb [24] and $CeCd_3P_3$ [58], indicating that the CEF effect plays a role.

The inverse magnetic susceptibility $[1/\chi(T)]$ curves are linear and parallel to each other from 200 to 300 K when $H_{\parallel c}$ and $H_{\parallel ab}$ are applied [Fig. 2(a)]. We fitted this region by using the Curie-Weiss (CW) law, $\chi(T) = C/(T - \theta_P)$, where $C = \frac{N_A \mu_{\rm eff}^2 \mu_B^2}{3k_B}$ and θ_P is the Weiss temperature. Here, $N_A = 6.02 \times 10^{23}$ mol^{-1} is Avogadro's number, $\mu_B = 9.274 \times 10^{-24}$ J/T is the Bohr magneton, and $k_B = 1.38 \times 10^{-23}$ J/K is the Boltzmann constant. The results are $\mu_{\rm eff}^c = 4.59\ \mu_B$ and $\theta_P^c = -47.55$ K for $H \parallel c$ axis and $\mu_{\rm eff}^{ab} = 4.54\ \mu_B$ and $\theta_P^{ab} = -4.75$ K for $H \parallel ab$ plane. The obtained effective moment agrees well with the value for the Hund's rule ground state of Yb^{3+}, $\mu_{\rm eff} = 4.54\ \mu_B$, again proving that the Yb ion is trivalent at high temperatures. The large difference between θ_P^c and θ_P^{ab} reflects large anisotropy, and we estimate the average Weiss temperature θ_P as $\theta_P = (\theta_P^c + 2\theta_P^{ab})/3 = -19$ K. The result is negative but much larger than the Weiss temperature for GdV_6Sn_6 (7.6 K) in magnitude [47]. This large, negative Weiss temperature is comparable to many Yb-based HF compounds [1].

The magnitude of the field-dependent magnetization $M(H)$ for $H \parallel ab$ plane is four times the magnitude of $M(H)$ for $H \parallel c$ axis at 2 K [Fig. 2(b)]. For $H \parallel ab$, $M(H)$ linearly

increases up to about 5 kOe, then shows a trend of saturation, and reaches 1.75 μ_B/Yb at 70 kOe, far less than the saturation moment of the Hund's rule ground state of Yb^{3+} (4.0 μ_B).

Figure 2(c) shows the specific heat for YbV_6Sn_6 and LuV_6Sn_6 from 1.8 to 10 K, presented as C_p/T versus T^2. As a nonmagnetic counterpart, the specific heat for LuV_6Sn_6 follows the relation $C_p(T) = \gamma T + \beta T^3$ at low temperatures, where γ equals 17.4 mJ mol^{-1} K^{-2} and the β value equals 0.000542 mJ mol^{-1} K^{-2}, which gives a Debye temperature Θ_D of 360 K. The γ value is slightly less than that in Ref. [48]. Assuming that γ mainly comes from vanadium, we notice that the value 2.9 mJ mol vanadium^{-1} K^{-2} is larger than that of regular metals such as gold and copper (<1 mJ mol^{-1} K^{-2}).

The low-temperature specific heat for YbV_6Sn_6 at zero field follows the relation $C_p(T) = \gamma T + \beta T^3$ from 3 to 10 K, with the same value of β as in LuV_6Sn_6. The γ value, estimated as 411 mJ mol^{-1} K^{-2}, meets the criteria for HF compounds (>400 mJ mol^{-1} K^{-2}) [1]. Below 3 K, C_p/T shows a pronounced increase as the temperature decreases. When a magnetic field is applied along the c-axis direction, the low-temperature C_p is significantly enhanced. A broad peak occurs at around 4 K when $H = 70$ kOe, and this peak shifts to higher temperatures in a stronger field. The significant change in C_p in the magnetic field indicates that a large part of the magnetic entropy below 2 K is released in an external field.

We compare the temperature-dependent resistivity $\rho(T)$ for YbV_6Sn_6 and LuV_6Sn_6 from 1.8 to 300 K in Fig. 2(d). The $\rho(T)$ curve for LuV_6Sn_6 has the profile of a normal metal. Its residual resistivity ρ_0 equals 15.3 μΩ cm, and its residual resistivity ratio RRR = ρ(300 K)/ρ(2 K) equals 6. The profile of the $\rho(T)$ curve for YbV_6Sn_6 is commonly observed in many HF compounds [20,21]. We used $\Delta\rho(T) = \rho_{Yb}(T) - \rho_{Lu}(T)$ to estimate the $4f$ part of the contribution, and the result is shown in the inset. $\Delta\rho$ exhibits a broad maximum at 30 K, which is likely due to Kondo coherence and the CEF effect [59]. The $-\log(T)$ dependence at high temperatures can be attributed to incoherent Kondo scattering in HF compounds. The resistivity is significantly suppressed in a magnetic field at low temperatures. Taken together, the magnetization, specific-heat, and resistivity properties demonstrate that a Kondo lattice of Yb ions takes a role in YbV_6Sn_6, but it enters neither an FL state nor a magnetic ordering state above 2 K.

C. Magnetic transition

To unveil the ground state of YbV_6Sn_6 at base temperature, we conducted heat capacity and resistance measurements below 2 K using a PPMS DR option. We applied magnetic fields along the c axis and in the ab plane. The zero-field specific heat displays a sharp λ-shaped peak at about 0.40 K, indicating an on-site second-order phase transition. When the temperature falls below 0.1 K, C_p exhibits an upturn due to the nuclear Schottky anomaly [Fig. 3(a)]. As shown in Figs. 3(a) and 4(a), the λ-shaped peak is suppressed by a magnetic field, and a broad peak replaces it when $H_{\|c} = 3$ kOe and $H_{\|ab} = 1$ kOe, respectively. In a stronger field, the peak shifts to higher temperatures and eventually becomes the feature we observed in Fig. 2(c) when $H_{\|c} \geqslant 70$ kOe. The insets of

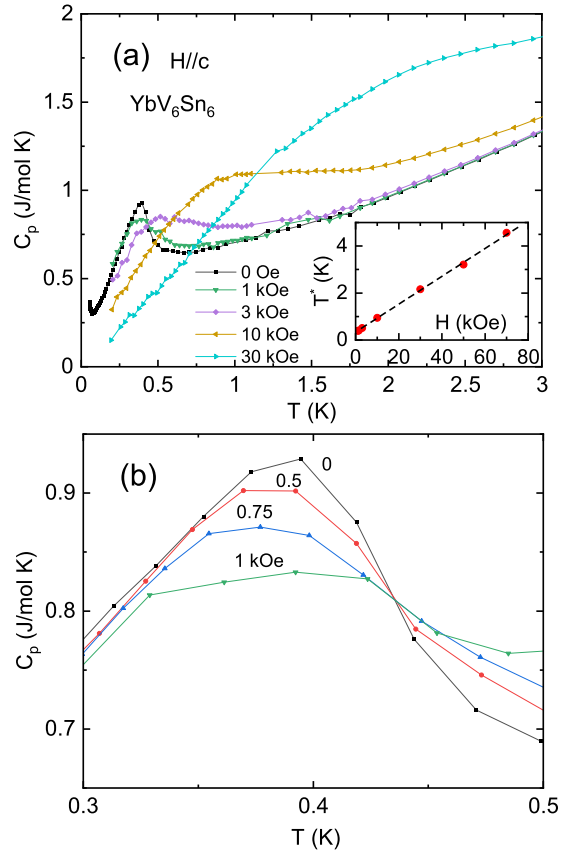

FIG. 3. Low-temperature specific heat for YbV_6Sn_6 for $H \parallel c$ axis. (a) Temperature-dependent specific heat in different magnetic fields. The λ-shaped peak at 0.4 K in zero field becomes a broad peak in nonzero field. Inset: the peak position (T^*) with respect to the field. (b) The λ-shaped peak changes into a broad peak in weak magnetic fields.

Figs. 3(a) and 4(a) show that the temperature of the C_p maximum (T^*) has a linear dependence on the field, with slopes of 0.059 and 0.272 K/kOe in $H_{\|c}$ and $H_{\|ab}$, respectively. The linear relation suggests that the broad peak observed in both directions is likely due to the Zeeman effect.

If we consider the broad peak as a two-level Schottky anomaly, the peak position satisfies the relation $k_BT^* = 0.42E_Z$, where $E_Z = 2MH$ is the Zeeman energy of the doublet in the field [13]. The estimated magnetic moments, $M^{\text{Zeeman}}_{H\|z} = 0.70\ \mu_B$ and $M^{\text{Zeeman}}_{H\perp z} = 3.23\ \mu_B$, are slightly larger than the calculated magnetization of a Kramers doublet ($M_{H\|z} = 0.57\ \mu_B$ and $M_{H\perp z} = 2.29\ \mu_B$, as shown below). Moreover, the linear extrapolation of the H dependence leads to an intercept field, $H = -5.7$ kOe for $H \parallel c$ axis and $H = -1.6$ kOe for $H \parallel ab$ plane. This negative intercept field implies an FM interaction that gives an additional effective field overlaying the external field. However, we tend to believe that the nature of the magnetic ordering at 0.4 K is AFM, as we will show below.

To check how the λ-shaped peak evolves into a broad peak in weak field, we conducted the measurements in fields of 500, 750, and 1000 Oe for $H \parallel c$ axis [Fig. 3(b)] and in fields of 100, 200, and 400 Oe for $H \parallel ab$ plane [Fig. 4(b)]. Despite the significant modification of the peak shape by the weak field,

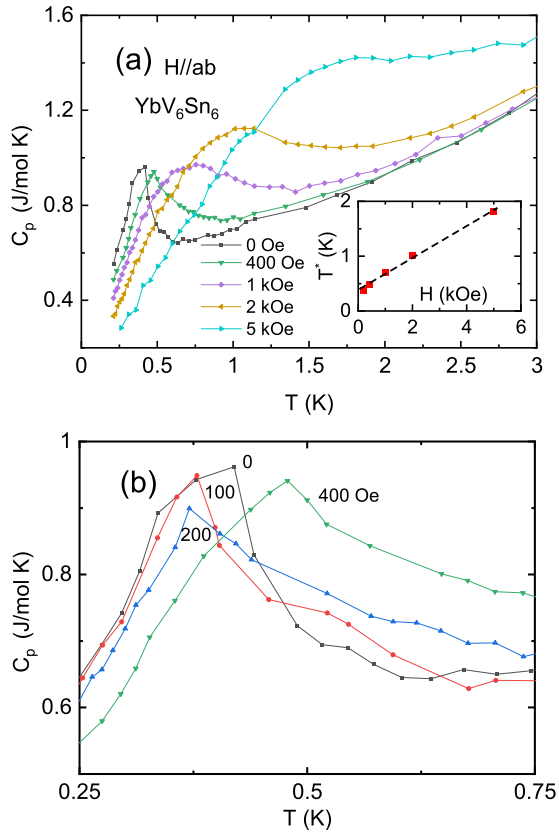

FIG. 4. Low-temperature specific heat for YbV_6Sn_6 for $H \parallel ab$ plane. (a) Temperature-dependent specific heat in different magnetic fields. The λ-shaped peak at 0.4 K in zero field becomes a broad peak in nonzero field. Inset: the peak position (T^*) with respect to the field. (b) The λ-shaped peak changes into a broad peak in weak magnetic fields.

the peak center position only shifts by less than 0.02 K toward zero. For a simple AFM-ordered, local-moment-bearing material, the peak should be suppressed to zero temperature by gradually increased magnetic field [60]. Our observation indicates that the magnetic ordering of YbV_6Sn_6 is not a simple AFM ordering of well-defined local moments. On the other hand, the specific-heat change for YbV_6Sn_6 in magnetic fields is similar to that of the HF compounds Ce_2NiSi_3 [61] and $Ce_5Ni_2Si_3$ [62]. The magnetic structures of these two HF compounds are sensitive to external magnetic field, and an FM alignment of magnetic moments can be easily induced by a weak field.

We subtracted the nuclear Schottky contribution $C_N(T)$, which is proportional to $1/T^2$, from C_p below 2 K. While the phonon contribution can be ignored at low temperatures, $\Delta C(T)/T$ remains unchanged below 0.4 K in zero field [Fig. 5(a)]. The low-temperature electronic specific-heat coefficient $\gamma = \Delta C(T)/T|_{T=0.2\,\mathrm{K}}$ was estimated as 2.5 J mol^{-1} K^{-2}. This value is much larger than the value we estimated in the temperature range 3–10 K and comparable to that of $YbRh_2Si_2$ [63]. The magnetic entropy S_m was inferred by integrating C_p/T when $H_{\parallel c} = 0$ and 50 kOe, after subtracting $C_N(T)$ at low temperatures and C_p/T of LuV_6Sn_6, which was treated as the phonon contribution. Noticing possible underestimation of S_m below 0.05 K that we cannot measure,

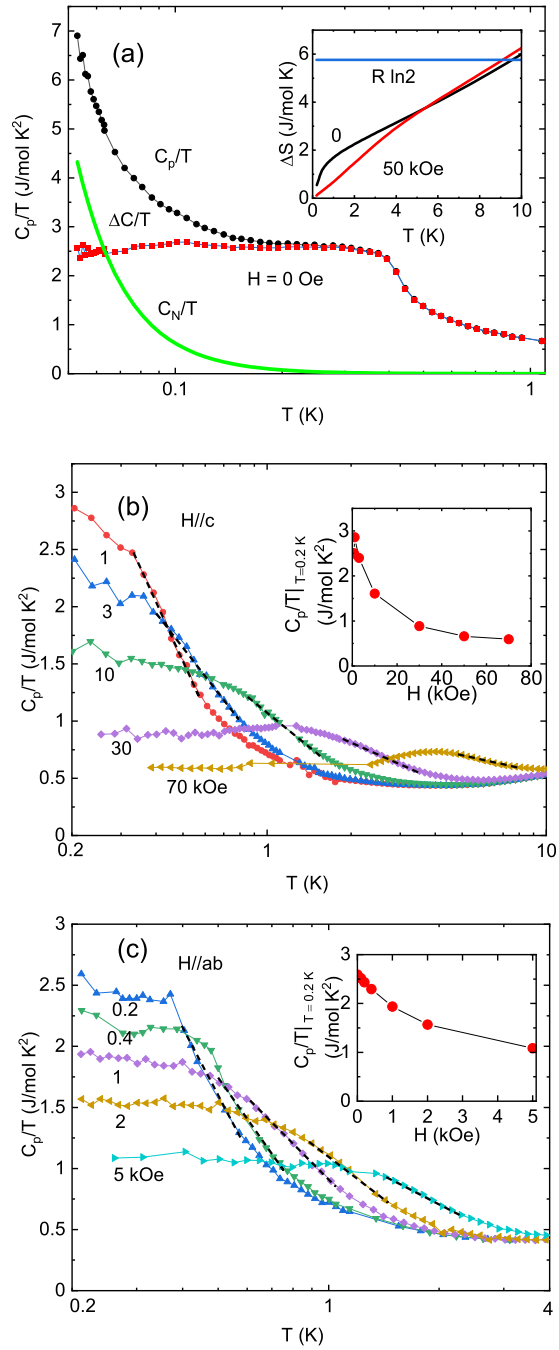

FIG. 5. Electronic specific heat of YbV_6Sn_6. (a) Low-temperature C/T in zero field, after subtracting the nuclear Schottky contribution. Inset: magnetic entropy ΔS_m below 10 K in $H = 0$ and 50 kOe for $H \parallel c$ axis. (b) C_p/T vs T in different magnetic fields for $H \parallel c$ axis. The dashed lines indicate the temperature region in which C_p/T shows $-\log(T)$ dependence. Inset: C_p/T at 0.2 K as a function of field. (c) C_p/T vs T in different magnetic fields for $H \parallel ab$ plane. The dashed lines indicate the temperature region in which C_p/T shows $-\log(T)$ dependence. Inset: C_p/T at 0.2 K as a function of field.

we find that only ∼15% of $R\ln(2)$ is released at T_N, where R is the gas constant, far less than the full magnetic entropy associated with a Kramers doublet. The Kondo temperature T_K can be estimated by $S_m(T = 0.5T_K) = 0.4R\ln(2)$ for a

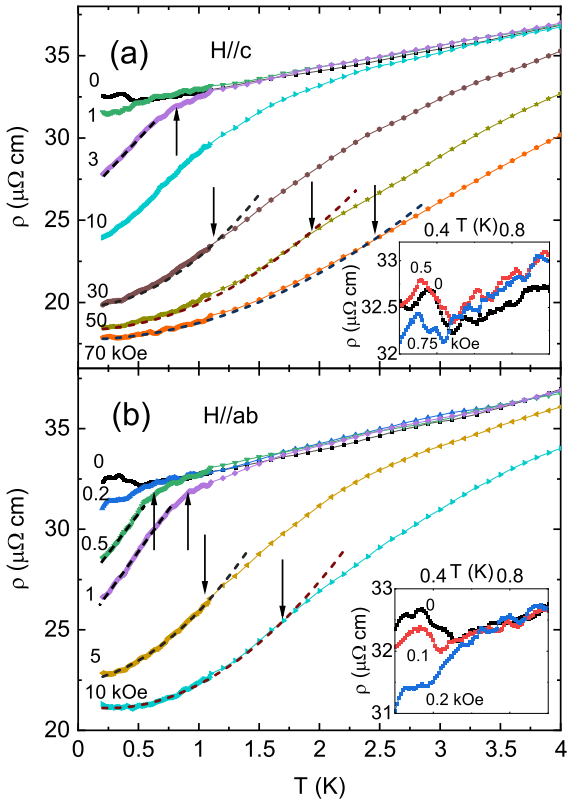

FIG. 6. Temperature-dependent resistivity in different magnetic fields. (a) $H \parallel c$ axis. (b) $H \parallel ab$ plane. The down arrows indicate the onset of Fermi-liquid behavior, while the up arrows indicate the knee points. The insets are zooms in weak fields.

doublet ground state [64]. Using this formula, we obtained a T_K value of 4.2 K. The inferred S_m recovers the full doublet entropy $R\ln(2)$ at 9 K and reaches $R\ln(4)$ at 28 K and $R\ln(8)$ at 45 K. When $H_{\parallel c} = 50$ kOe, S_m is released more slowly below 2 K, but slightly faster above 2 K, and also recovers $R\ln(2)$ at 9 K.

Figure 5(b) shows $C_p(T)/T$ in different $H_{\parallel c}$ from 0.2 to 10 K. Please note that the nuclear Schottky anomaly and phonon contribution can be ignored in this temperature range. When $H_{\parallel c} \leqslant 10$ kOe, $C_p(T)/T$ continuously increases as the temperature decreases to 0.2 K. The low-temperature value of $C_p(T)/T$ drops in higher fields and becomes invariant with respect to temperature when $H_{\parallel c} \geqslant 30$ kOe, indicating an FL ground state. The inset shows the $C_p(T)/T$ values at 0.2 K with respect to the field, which can be treated as the γ values. The $C_p(T)/T$ values are in general much larger than 400 mJ mol^{-1} K^{-2}, again indicating that the electron mass was seriously underestimated according to the data from 3 to 10 K in zero field.

Figure 5(c) shows $C_p(T)/T$ in different $H_{\parallel ab}$ from 0.2 to 4 K. Here the profile is similar to that for $H_{\parallel c}$, but the magnetic field is much weaker. The low-temperature value of $C_p(T)/T$ becomes invariant with respect to temperature when $H_{\parallel ab} \geqslant 2$ kOe, indicating that a field-driven FL ground state is more easily accessible.

Figures 6(a) and 6(b) display $\rho(T)$ for YbV_6Sn_6 in magnetic fields applied along the c axis and in the ab plane, respectively. The zero-field $\rho(T)$ decreases linearly with temperature, reaching a minimum at 0.4 K, and then shows a rise on site. We compare the $\rho(T)$ for GdV_6Sn_6, which exhibits magnetic ordering of well-defined local moments associated with Gd^{3+} ions at 5.0 K [47]. The $\rho(T)$ of GdV_6Sn_6 is similar to that of LuV_6Sn_6 above 5 K and then shows a slight drop below the ordering temperature, which is most likely due to a loss of spin disorder scattering of the conduction electrons. Indeed, the $\rho(T)$ of RV_6Sn_6 (R = Gd–Ho) in general drops less than 0.5 μΩ cm from their magnetic ordering temperature to the base temperature [48]. This $\rho(T)$ drop has much smaller magnitude than the $\rho(T)$ rise of YbV_6Sn_6.

On the other hand, the profile of $\rho(T)$ for YbV_6Sn_6 is similar to that for YbPtBi [20], a classical HF system which shows AFM ordering at 0.4 K. The rise in $\rho(T)$ is a general signature of charge density wave (CDW) transition, of spin density wave (SDW) transition, and of AFM transition which opens a superzone gap. It is noteworthy that our sample was mounted on the DR cold stage with GE varnish. As explained in Ref. [20], mounting YbPtBi samples with GE varnish can bring local strain, which weakens the rise in $\rho(T)$ during the transition. This is possibly due to the different thermal contraction between the sample and the cold stage, causing stress. It is likely that a similar effect exists in YbV_6Sn_6, and this requires further investigation.

We notice that $\rho(T)$ is very sensitive to the fields below 0.4 K: $H_{\parallel ab}$ of 200 Oe and $H_{\parallel c}$ of 1 kOe can fully suppress the rise. In moderate fields $H_{\parallel ab}$ of 1 kOe and $H_{\parallel c}$ of 3 kOe, the resistivity remains intact above 1 K but significantly drops at lower temperatures. This unusual behavior leads to a "knee point" on the $\rho(T)$ curve (shown as up arrows), below and above which $\rho(T)$ quasilinearly increases with different slopes. The $\rho(T)$ curves show T^2 dependence at low temperatures when $H_{\parallel ab}$ and $H_{\parallel c}$ are stronger than 5 and 30 kOe, respectively. The down arrows in Fig. 6 indicate the onset of Fermi-liquid behavior. Similar to HF compounds near the magnetic instability [65], the magnetic field strongly suppresses the residual resistivity ρ_0 of YbV_6Sn_6.

D. Non-Fermi liquid

When a moderate field suppressed the phase transition, we observed a linear power law $\rho(T) \propto T$ at low temperatures (Fig. 6), which is a feature of NFLs. As the knee points are below 1 K in general, the linear $\rho(T)$ only extends to a very limited temperature range. This feature is unlike what was observed in $YbRh_2Si_2$, where $\rho(T)$ linearly extends to about 20 K above the field-induced QCP [59]. On the other hand, $C_p(T)/T$ for YbV_6Sn_6 only shows $-\log(T)$ dependence in a limited temperature range [see dashed lines in Figs. 5(b) and 5(c)]. These observations demonstrate that YbV_6Sn_6 can enter a quantum critical region when the transition is suppressed by a magnetic field.

To further elaborate the transition and field-induced quantum criticality, we conducted dc magnetization measurements from 1.8 to 0.4 K (field cooling) when $H \parallel ab$ plane. At the lowest temperature (0.4 K), the inverse magnetic susceptibility [$1/\chi(T) = H/M$] apparently deviates from the CW law [Fig. 7(a)], indicating a nearby magnetic transition. Plotting M/H with respect to $\log(T)/T$, $T^{-3/2}$, and $T^{-4/3}$ when $H_{\parallel ab}$

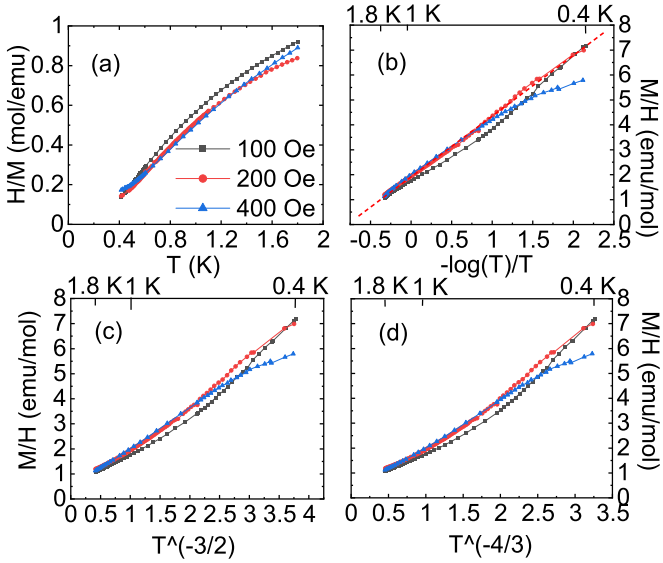

FIG. 7. Low-temperature magnetization. (a) H/M as a function of T. (b), (c), and (d) M/H as a function of $-\log(T)/T$, $T^{-3/2}$, and $T^{-4/3}$, respectively.

is 100, 200, and 400 Oe, we notice that χ is linearly dependent on $\log(T)/T$ [Fig. 7(b)] in 200 Oe, which is the critical field suppressing the transition exactly, according to the $\rho(T)$ measurement. The dependence of $-\log(T)/T$ for χ is consistent with Moriya's model for the QCP in AFM two-dimensional (AFM-2D) systems [2]. The power laws for the QCP in AFM-3D ($\chi \propto T^{-3/2}$) and FM-3D systems ($\chi \propto T^{-4/3}$) do not cover our observation [Figs. 7(c) and 7(d)].

IV. ANALYSIS AND DISCUSSION

The CEF leads the anisotropic $\chi(T)$ which has a similar profile to the $\chi(T)$ for TmV_6Sn_6 and ErV_6Sn_6 [48,49]. As the Yb^{3+} is located in hexagonal coordination, the CEF Hamiltonian is given as $\mathcal{H}_{\rm CEF} = B_2^0O_2^0 + B_4^0O_4^0 + B_6^0O_6^0 + B_6^6O_6^6$, where B_n^m are CEF parameters and O_n^m are Stevens operators [66]. The existence of B_6^6 leads to a mix between $|\pm\frac{7}{2}\rangle$ and $|\mp\frac{5}{2}\rangle$ and thus gives rise to two new doublets.

$$|\Gamma_{\rm mix,1}\rangle = \cos\alpha|\pm 7/2\rangle + \sin\alpha|\mp 5/2\rangle,$$
$$|\Gamma_{\rm mix,2}\rangle = \sin\alpha|\pm 7/2\rangle - \cos\alpha|\mp 5/2\rangle,$$
$$|\Gamma_{3/2}\rangle = |\pm 3/2\rangle, \quad |\Gamma_{1/2}\rangle = |\pm 1/2\rangle.$$

The formula for the CEF magnetic susceptibility $\chi_{\rm CEF}$ is given by

$$\chi_{\rm CEF} = \frac{2N_Ag_J^2\mu_B^2\mu_0}{Z}\left[\sum_n \beta|\langle J_{i,n}\rangle|^2 e^{-\beta E_n} + 2\sum_{m\neq n}|\langle m|J_{i,n}|n\rangle|^2\left(\frac{e^{-\beta E_m} - e^{-\beta E_n}}{E_n - E_m}\right)\right]$$

with $\beta = 1/k_BT$, $Z = 2\Sigma_n e^{-\beta E_n}$, $i = x, z$, and $n, m = 0, 1, 2, 3$. Here, z is the quantization axis. The first term is the Curie contribution to the paramagnetic susceptibility, and the second term is the Van Vleck susceptibility [67]. Considering the anisotropic molecular field parameters λ_α, the total inverse magnetic susceptibility is given by $1/\chi_\alpha = 1/\chi_{\rm CEF} - \lambda_\alpha$ [68]. We determined all the CEF parameters by fitting the magnetic susceptibility data in Fig. 2(a), and these parameters are listed in Table I. The purple curves in Fig. 2(a) represent the fitting curves.

TABLE I. Crystalline-electric-field parameters for YbV_6Sn_6. According to our fitting results, the doublet $|\Gamma_{1/2}\rangle = |\pm 1/2\rangle$ is chosen as the ground state with $E_0 = 0$.

CEF parameters	Energy separations	Mixing angle
$B_2^0 = 4.90$ K	$\Delta_1 = 28.66$ K	$\alpha = 1.57^\circ$
$B_4^0 = 1.00 \times 10^{-3}$ K	$\Delta_2 = 86.87$ K	
$B_6^0 = -1.00 \times 10^{-6}$ K	$\Delta_3 = 176.27$ K	
$B_6^6 = -9.63 \times 10^{-6}$ K		
$\lambda_{ab} = -6.0$ mol/emu		
$\lambda_c = -0.5$ mol/emu		

In the presence of a CEF, the eightfold degeneracy of the Yb^{3+} ion is lifted and split into four Kramers doublets. The energy separations between the excited states and the ground state are designated as Δ_1, Δ_2, and Δ_3. A schematic illustration of CEF splitting is presented in Fig. 8. We notice that the CEF splitting is larger than the estimation from the magnetic specific heat, which may be due to the uncertainty of the heat capacity measurement at high temperatures. The Kramers doublet $|\Gamma_{1/2}\rangle = |\pm 1/2\rangle$ is determined as the CEF ground state, and the calculated saturated magnetizations parallel and perpendicular to the c axis are

$$M_{H\|z} = \langle\Gamma_{\frac{1}{2},1}|J_z|\Gamma_{\frac{1}{2},1}\rangle g_J\mu_B = 0.5(8/7)\mu_B = 0.57\mu_B,$$
$$M_{H\perp z} = \langle\Gamma_{\frac{1}{2},1}|J_x|\Gamma_{\frac{1}{2},1}\rangle g_J\mu_B = 2(8/7)\mu_B = 2.29\mu_B.$$

The calculated $M_{H\|z}$ is a quarter of $M_{H\perp z}$, which is consistent with the anisotropy of $M(H)$ curves at 2 K [Fig. 2(b)]. The value of $M_{H\|z}$ is close to M at 2 K in 70 kOe (0.4 μ_B/Yb) as well. Thus we conclude that YbV_6Sn_6 hosts a triangular Kondo lattice in which the effective spin of the Kramers doublet is $J_{\rm eff} = 1/2$.

We now try to understand the ground state of YbV_6Sn_6 in various magnetic fields. When $H_{\|c} \geqslant 30$ kOe and $H_{\|ab} \geqslant 6$ kOe, respectively, $C_p/T = \gamma$ is invariant at low temperatures while $\rho(T)$ shows T^2 dependence concomitantly, which explicitly points to an FL ground state. We obtained the co-

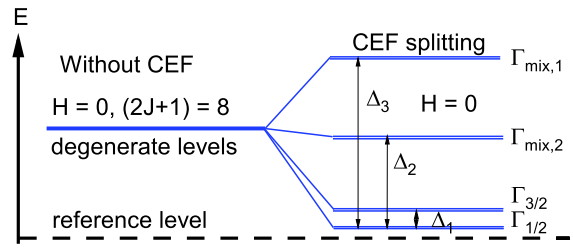

FIG. 8. Proposed CEF scheme for YbV_6Sn_6 with $\Delta_1 = 28.66$ K, $\Delta_2 = 86.87$ K, and $\Delta_3 = 176.27$ K.

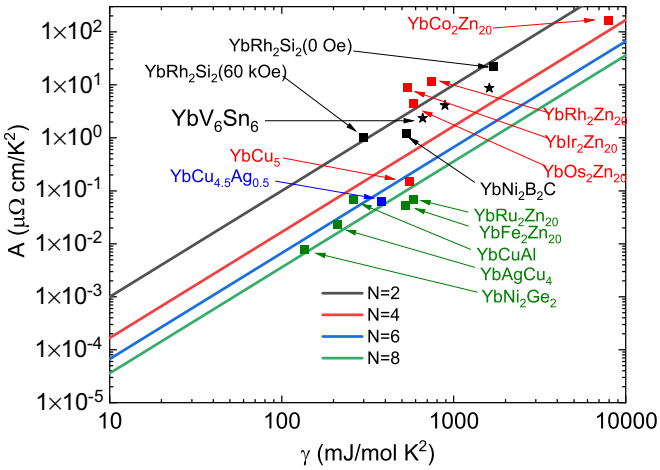

FIG. 9. Log-log plot of A vs γ. Three sets of YbV_6Sn_6 data for $H = 10$, 30, and 50 kOe are represented as the stars from upper right to bottom left, respectively. The values for other representative Yb-based compounds are from Refs. [59,63,69–73] and the references therein.

efficient A by fitting the data of $\rho(T) = \rho_0 + AT^2$ in the FL state and then plotted it as a function of γ when $H_{\|c} = 30$, 50, and 70 kOe. The plot, known as a Kadowaki-Woods (KW) plot [74] (Fig. 9), has included other Yb-based HF compounds which have different degenerated ground states. The points for YbV_6Sn_6 are close to the line of $N = 2$, implying that the Kondo screening acts on the Kramers doublet state for Yb^{3+}, consistent with our analysis of the CEF. The heaviness of the effective electron mass of YbV_6Sn_6 is highlighted although it has been strongly suppressed by the magnetic field.

The heavy effective electron mass indicates that the Kondo temperature T_K is extremely low for YbV_6Sn_6. We estimate T_K by using the formula $T_K = R\ln(N)/\gamma$, where N is the degeneracy ($N = 2$ for Yb^{3+}), R is the gas constant, and γ is the coefficient of specific heat. From Fig. 5, we take $\gamma = 2.5\ \mathrm{J\,mol^{-1}\,K^{-2}}$ leading to a T_K value of 2.3 K, smaller than the 4.2 K which is estimated from the magnetic entropy. We think that the T_K value of 4.2 K is closer to the observed behavior, e.g., an enhanced γ value in the specific heat is reported below 4 K and originates from the Kondo effect. Considering that the CEF energy separation between the ground state and other states is larger than 30 K, YbV_6Sn_6 can be classified as an ordinary HF system which shows a Kramers doublet before it enters a Kondo screening state when cooling down.

Based on the $\rho(T)$ data in various magnetic fields, we plot a coarse T-H phase diagram for YbV_6Sn_6 when $H \| c$ axis and $H \| ab$ plane in Figs. 10(a) and 10(b), respectively. When the magnetic ordering is suppressed by H, we observe a linear dependence of $\rho(T)$, a characteristic feature of an NFL. However, currently, it is not clear whether the NFL region reduces to a QCP or remains a finite range in the H axis at zero temperature. In other words, we do not know whether the FL region connects with the AFM region at a QCP in zero temperature, like the phase diagram in $YbRh_2Si_2$ [75], or detaches from it, like the observed diagrams for YbAgGe [21] and Ge-doped $YbRh_2Si_2$ [76].

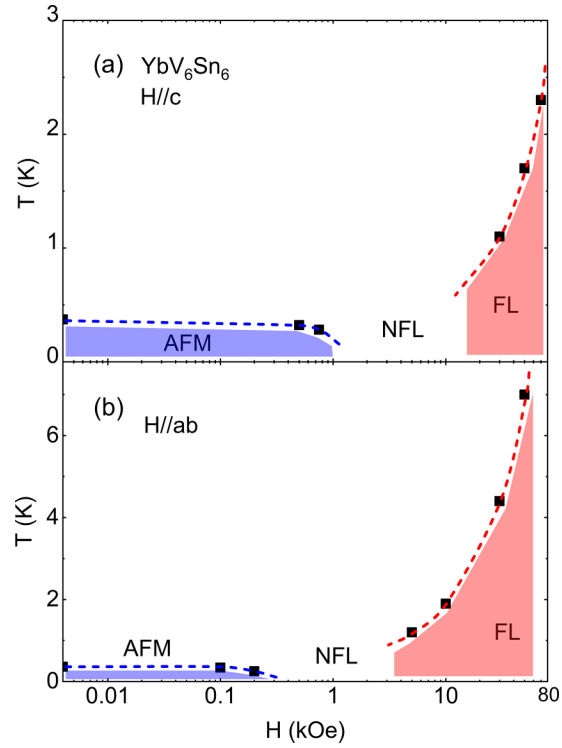

FIG. 10. A coarse T-H phase diagram of YbV_6Sn_6 when (a) $H \| c$ axis and (b) $H \| ab$ plane. H is plotted on a log scale.

Finally, we discuss the phase transition at 0.40 K in zero field and envisage possible ground states for YbV_6Sn_6. The dilute R concentration and the long R-R distances are highlighted in the "166" family, and we expect weak RKKY interaction and low magnetic ordering temperature for R moments. For dilute Yb-based HF compounds such as YbT_2Zn_{20} (T = Fe, Co, Ru, Rh, Os, Ir), the Kondo effect in general prevails and leads to a heavy FL ground state with no magnetic ordering down to 20 mK [73]. As other RV_6Sn_6 compounds show extremely low magnetic ordering temperatures [48,49], we infer that the RKKY interaction in YbV_6Sn_6 is very weak, because Yb has the smallest de Gennes factor (dG = 0.32) which scales with the strength of the RKKY interaction. If the de Gennes scaling plays a role in the magnetic ordering in RV_6Sn_6, the T_N for YbV_6Sn_6 shall be below 0.1 K because GdV_6Sn_6 has $T_N = 5.0$ K and dG = 15.75. Recent studies showed that the T_N's for R = Gd–Ho approximately follow the de Gennes scaling while ErV_6Sn_6 and TmV_6Sn_6 show no magnetic ordering down to 1.8 K [48,49]. The high $T_N = 0.40$ K in YbV_6Sn_6 is unexpected, because both the Kondo effect and geometrical frustration in a triangular lattice shall impede the long-range order and suppress the T_N instead of enhancing it.

Because we lack magnetization measurements below 0.40 K at this point, we can only infer the nature of the phase transition based on specific-heat and resistivity data. Firstly, we can rule out the possibility of a spin glass state based on the specific-heat data. The $C_p(T)$ of a classical spin glass system manifests a broad peak around the spin freezing temperature, and the low-temperature specific heat follows a T^n dependence ($n \geqslant 1$), which is quite robust under magnetic

fields [77]. In comparison, the $C_p(T)$ of YbV_6Sn_6 shows a typical λ-shaped peak for the second-order transition, and the γ value is easily suppressed by the magnetic field. So far, no evidence for the existence of spin glass ordering has been found in other RV_6Sn_6 compounds [48,49].

A simple FM ordering is not likely the nature of the transition either. The Weiss temperatures of YbV_6Sn_6 are negative in both directions, indicating that an AFM interaction prevails. Irrespective of the magnetic field direction, the magnetic order in YbV_6Sn_6 is suppressed by the presence of a magnetic field, which is a common behavior in antiferromagnets. The susceptibility for $H \parallel ab$ plane follows a $-\log(T)/T$ dependence slightly when a field-driven QCP occurs, and the power law corresponds to the QCP of the AFM ordering in 2D systems.

Noticing that the zero-field $\rho(T)$ shows a rise on site, similar to what was observed in YbPtBi [20], it is plausible that there exists an SDW-type AFM ordering which may partially gap the Fermi surface. In a global phase diagram of HF compounds, YbPtBi represents the system that goes from a small Fermi surface of AFM phase (AFM_S) to a large Fermi surface of paramagnetic phase (P_L), passing through a small Fermi surface of paramagnetic phase (P_S). A P_S phase often corresponds to spin-Peierls order, which contains a spin gap. On the other hand, the SDW order of HF quasiparticles of the P_L phase [33] can also cause a magnetic gap. It is not clear what the position of YbV_6Sn_6 in the global phase diagram is or what the nature of the AFM transition is. Further studies on the Hall effect and magnetoresistance in extremely low temperatures will unveil whether and when the Fermi surface is reconstructed in a magnetic field. Below, we discuss the possibility of exotic magnetic ground states based on previous theoretical works on the triangular Kondo lattice model.

In a local-moment-bearing triangular lattice, the frustration can be overcome in a 120° magnetic structure of the in-plane moments [31]. However, in a triangular Kondo lattice, the frustration can be resolved by forming more exotic quantum states. Theoretical studies suggested that in a 2D triangular Kondo lattice, various quantum states can emerge, from the chiral magnetic ordering of the local moments [78] to a PKS state [31,32]. The latter has been found experimentally in the Ce-based distorted kagome lattice in CePdAl [11] and the U-based triangular lattice in UNi_4B [79]. In a PKS state, the 2D triangular Kondo lattice resolves the frustration by means of forming a subset of nonmagnetic Kondo singlet sites while the remaining magnetic sites form an AFM honeycomb lattice. If a similar PKS state exists in YbV_6Sn_6 in zero field, the magnetic ordering may be largely different from that in other members of the RV_6Sn_6 family, and the breaking of the de Gennes scaling is not unexpected.

Besides a PKS state, a triangular Kondo lattice can also give rise to complex chiral spin structures and even potentially host a skyrmion phase [78,80]. Recent studies on GdV_6Sn_6 suggested the existence of a noncollinear spin structure below its T_N [47]. The triangular Kondo lattice in YbV_6Sn_6 may also resolve the frustration by forming those unusual magnetic structures in the manner of the local moment. Future studies such as ones involving magnetization measurement and neutron scattering below 0.40 K will help to solve the puzzle.

Recent studies on ScV_6Sn_6 discovered a remarkable CDW transition at 92 K [81] in which the vanadium electrons in a kagome layer play a key role. It remains an open question whether the vanadium atoms play a role in the magnetic properties of YbV_6Sn_6.

V. CONCLUSIONS

The magnetization, specific heat, and resistivity for single crystals of YbV_6Sn_6 show typical physical properties of HF compounds, while a remarkable magnetic ordering occurs at 0.40 K. When the ordering is suppressed by a weak magnetic field, we observed characteristic behaviors of an NFL, including a linear T-dependent resistivity, $-\log(T)/T$ scale of magnetic susceptibility, and $-\log(T)$ scale of C_p/T. YbV_6Sn_6 is represented as a rare example of the HF compounds bearing a Yb-based triangular Kondo lattice, while its magnetic ground state needs further elaboration. YbV_6Sn_6 has the potential to be a model system for exploring the exotic quantum states of triangular lattices and understanding the global phase diagram of HF compounds.

ACKNOWLEDGMENTS

We gratefully thank Nanlin Wang, Yuan Li, Yi Zhang, Peijie Sun, and H. Q. Yuan for discussions. This work was supported by the National Key Research and Development Program of China (Grant No. 2021YFA1401902), the CAS Interdisciplinary Innovation Team, the Strategic Priority Research Program of Chinese Academy of Sciences (Grant No. XDB28000000), and the National Natural Science Foundation of China (Grants No. 12141002, No. 12225401, and No. U1832214).

[1] G. R. Stewart, Rev. Mod. Phys. **56**, 755 (1984).
[2] G. R. Stewart, Rev. Mod. Phys. **73**, 797 (2001).
[3] P. Coleman, in *Handbook of Magnetism and Advanced Magnetic Materials*, edited by H. Kronmüller and S. Parkin (Wiley, New York, 2007), pp. 95–148.
[4] P. Gegenwart, Q. Si, and F. Steglich, Nat. Phys. **4**, 186 (2008).
[5] S. Paschen and Q. Si, Nat. Rev. Phys. **3**, 9 (2021).
[6] H. Q. Yuan, F. M. Grosche, M. Deppe, C. Geibel, G. Sparn, and F. Steglich, Science **302**, 2104 (2003).
[7] H. R. Ott, H. Rudigier, Z. Fisk, and J. L. Smith, Phys. Rev. Lett. **50**, 1595 (1983).
[8] B. Shen, Y. Zhang, Y. Komijani, M. Nicklas, R. Borth, A. Wang, Y. Chen, Z. Nie, R. Li, X. Lu, H. Lee, M. Smidman, F. Steglich, P. Coleman, and H. Q. Yuan, Nature (London) **579**, 51 (2020).
[9] S. Doniach, Phys. B+C (Amsterdam) **91**, 231 (1977).
[10] M. Vojta, Rep. Prog. Phys. **81**, 064501 (2018).
[11] A. Dönni, G. Ehlers, H. Maletta, P. Fischer, H. Kitazawa, and M. Zolliker, J. Phys.: Condens. Matter **8**, 11213 (1996).

[12] J. Zhang, H. Zhao, M. Lv, S. Hu, Y. Isikawa, Y.-f. Yang, Q. Si, F. Steglich, and P. Sun, Phys. Rev. B **97**, 235117 (2018).

[13] S. Lucas, K. Grube, C.-L. Huang, A. Sakai, S. Wunderlich, E. L. Green, J. Wosnitza, V. Fritsch, P. Gegenwart, O. Stockert, and H. v. Löhneysen, Phys. Rev. Lett. **118**, 107204 (2017).

[14] Y. Tokiwa, C. Stingl, M. S. Kim, T. Takabatake, and P. Gegenwart, Sci. Adv. **1**, e1500001 (2015).

[15] Q. Si, Phys. B (Amsterdam) **378-380**, 23 (2006).

[16] P. Coleman and A. H. Nevidomskyy, J. Low Temp. Phys. **161**, 182 (2010).

[17] Q. Si, J. H. Pixley, E. Nica, S. J. Yamamoto, P. Goswami, R. Yu, and S. Kirchner, J. Phys. Soc. Jpn. **83**, 061005 (2014).

[18] S. Nakatsuji, K. Kuga, Y. Machida, T. Tayama, T. Sakakibara, Y. Karaki, H. Ishimoto, S. Yonezawa, Y. Maeno, E. Pearson, G. G. Lonzarich, L. Balicas, H. Lee, and Z. Fisk, Nat. Phys. **4**, 603 (2008).

[19] E. Schuberth, M. Tippmann, L. Steinke, S. Lausberg, A. Steppke, M. Brando, C. Krellner, C. Geibel, R. Yu, Q. Si, and F. Steglich, Science **351**, 485 (2016).

[20] E. D. Mun, S. L. Bud'ko, C. Martin, H. Kim, M. A. Tanatar, J.-H. Park, T. Murphy, G. M. Schmiedeshoff, N. Dilley, R. Prozorov, and P. C. Canfield, Phys. Rev. B **87**, 075120 (2013).

[21] S. L. Bud'ko, E. Morosan, and P. C. Canfield, Phys. Rev. B **69**, 014415 (2004).

[22] Q. Si and F. Steglich, Science **329**, 1161 (2010).

[23] L. Balents, Nature (London) **464**, 199 (2010).

[24] M. S. Kim, M. C. Bennett, and M. C. Aronson, Phys. Rev. B **77**, 144425 (2008).

[25] M. S. Kim and M. C. Aronson, J. Phys.: Condens. Matter **23**, 164204 (2011).

[26] M. S. Kim and M. C. Aronson, Phys. Rev. Lett. **110**, 017201 (2013).

[27] J. A. Paddison, M. Daum, Z. Dun, G. Ehlers, Y. Liu, M. Stone, H. Zhou, and M. Mourigal, Nat. Phys. **13**, 117 (2017).

[28] M. M. Bordelon, E. Kenney, C. Liu, T. Hogan, L. Posthuma, M. Kavand, Y. Lyu, M. Sherwin, N. P. Butch, C. Brown, M. J. Graf, L. Balents, and S. D. Wilson, Nat. Phys. **15**, 1058 (2019).

[29] I. Martin and C. D. Batista, Phys. Rev. Lett. **101**, 156402 (2008).

[30] Y. Kato, I. Martin, and C. D. Batista, Phys. Rev. Lett. **105**, 266405 (2010).

[31] Y. Motome, K. Nakamikawa, Y. Yamaji, and M. Udagawa, Phys. Rev. Lett. **105**, 036403 (2010).

[32] K. Noda, T. Yoshida, R. Peters, and N. Kawakami, JPS Conf. Proc. **3**, 014019 (2014).

[33] Q. Si, Phys. Status Solidi B **247**, 476 (2010).

[34] M. Keßler and R. Eder, Phys. Rev. B **102**, 235125 (2020).

[35] J.-X. Yin, W. Ma, T. A. Cochran, X. Xu, S. S. Zhang, H.-J. Tien, N. Shumiya, G. Cheng, K. Jiang, B. Lian, Z. Song, G. Chang, I. Belopolski, D. Multer, M. Litskevich, Z.-J. Cheng, X. P. Yang, B. Swidler, H. Zhou, H. Lin *et al.*, Nature (London) **583**, 533 (2020).

[36] W. Ma, X. Xu, J.-X. Yin, H. Yang, H. Zhou, Z.-J. Cheng, Y. Huang, Z. Qu, F. Wang, M. Z. Hasan, and S. Jia, Phys. Rev. Lett. **126**, 246602 (2021).

[37] Y. Ishii, H. Harima, Y. Okamoto, J.-i. Yamaura, and Z. Hiroi, J. Phys. Soc. Jpn. **82**, 023705 (2013).

[38] M. Li, Q. Wang, G. Wang, Z. Yuan, W. Song, R. Lou, Z. Liu, Y. Huang, Z. Liu, H. Lei, Z. Yin, and S. Wang, Nat. Commun. **12**, 3129 (2021).

[39] S. Peng, Y. Han, G. Pokharel, J. Shen, Z. Li, M. Hashimoto, D. Lu, B. R. Ortiz, Y. Luo, H. Li, M. Guo, B. Wang, S. Cui, Z. Sun, Z. Qiao, S. D. Wilson, and J. He, Phys. Rev. Lett. **127**, 266401 (2021).

[40] X. Xu, J.-X. Yin, W. Ma, H.-J. Tien, X.-B. Qiang, P. V. S. Reddy, H. Zhou, J. Shen, H.-Z. Lu, T.-R. Chang, Z. Qu, and S. Jia, Nat. Commun. **13**, 1197 (2022).

[41] T. Mazet, H. Ihou-Mouko, D. H. Ryan, C. J. Voyer, J. M. Cadogan, and B. Malaman, J. Phys.: Condens. Matter **22**, 116005 (2010).

[42] T. Mazet, D. Malterre, M. François, C. Dallera, M. Grioni, and G. Monaco, Phys. Rev. Lett. **111**, 096402 (2013).

[43] L. Eichenberger, D. Malterre, B. Malaman, and T. Mazet, Phys. Rev. B **96**, 155129 (2017).

[44] A. Weiland, L. J. Eddy, G. T. McCandless, H. Hodovanets, J. Paglione, and J. Y. Chan, Cryst. Growth Des. **20**, 6715 (2020).

[45] M. A. Avila, T. Takabatake, Y. Takahashi, S. L. Bud'ko, and P. C. Canfield, J. Phys.: Condens. Matter **17**, 6969 (2005).

[46] L. Romaka, Y. Stadnyk, V. V. Romaka, P. Demchenko, M. Stadnyshyn, and M. Konyk, J. Alloys Compd. **509**, 8862 (2011).

[47] G. Pokharel, S. M. L. Teicher, B. R. Ortiz, P. M. Sarte, G. Wu, S. Peng, J. He, R. Seshadri, and S. D. Wilson, Phys. Rev. B **104**, 235139 (2021).

[48] J. Lee and E. D. Mun, Phys. Rev. Mater. **6**, 083401 (2022).

[49] X. Zhang, Z. Liu, Q. Cui, Q. Guo, N. Wang, L. Shi, H. Zhang, W. Wang, X. Dong, J. Sun, Z. Dun, and J. Cheng, Phys. Rev. Mater. **6**, 105001 (2022).

[50] E. Rosenberg, J. M. DeStefano, Y. Guo, J. S. Oh, M. Hashimoto, D. Lu, R. J. Birgeneau, Y. Lee, L. Ke, M. Yi, and J.-H. Chu, Phys. Rev. B **106**, 115139 (2022).

[51] G. Pokharel, B. R. Ortiz, J. Chamorro, P. Sarte, L. Kautzsch, G. Wu, J. Ruff, and S. D. Wilson, Phys. Rev. Mater. **6**, 104202 (2022).

[52] P. C. Canfield, T. Kong, U. S. Kaluarachchi, and N. H. Jo, Philos. Mag. **96**, 84 (2016).

[53] D. C. Fredrickson, S. Lidin, G. Venturini, B. Malaman, and J. Christensen, J. Am. Chem. Soc. **130**, 8195 (2008).

[54] T.-M. Gesing, R. Pöttgen, W. Jeitschko, and U. Wortmann, J. Alloys Compd. **186**, 321 (1992).

[55] K. Hara, S. Matsuda, E. Matsuoka, K. Tanigaki, A. Ochiai, S. Nakamura, T. Nojima, and K. Katoh, Phys. Rev. B **85**, 144416 (2012).

[56] A. Iandelli, J. Less-Common Met. **90**, 121 (1983).

[57] B. Gibson, R. Pöttgen, R. K. Kremer, A. Simon, and K. R. A. Ziebeck, J. Alloys Compd. **239**, 34 (1996).

[58] J. Lee, A. Rabus, N. R. Lee-Hone, D. M. Broun, and E. D. Mun, Phys. Rev. B **99**, 245159 (2019).

[59] O. Trovarelli, C. Geibel, S. Mederle, C. Langhammer, F. M. Grosche, P. Gegenwart, M. Lang, G. Sparn, and F. Steglich, Phys. Rev. Lett. **85**, 626 (2000).

[60] O. Trovarelli, C. Geibel, R. Cardoso, S. Mederle, R. Borth, B. Buschinger, F. M. Grosche, Y. Grin, G. Sparn, and F. Steglich, Phys. Rev. B **61**, 9467 (2000).

[61] M. Szlawska and D. Kaczorowski, Phys. Rev. B **85**, 134423 (2012).

[62] B. K. Lee, D. H. Ryu, D. Y. Kim, J. B. Hong, M. H. Jung, H. Kitazawa, O. Suzuki, S. Kimura, and Y. S. Kwon, Phys. Rev. B **70**, 224409 (2004).

[63] P. Gegenwart, J. Custers, C. Geibel, K. Neumaier, T. Tayama, K. Tenya, O. Trovarelli, and F. Steglich, Phys. Rev. Lett. **89**, 056402 (2002).
[64] S. Kirchner, S. Paschen, Q. Chen, S. Wirth, D. Feng, J. D. Thompson, and Q. Si, Rev. Mod. Phys. **92**, 011002 (2020).
[65] J. Flouquet, P. Haen, F. Lapierre, C. Fierz, A. Amato, and D. Jaccard, J. Magn. Magn. Mater. **76-77**, 285 (1988).
[66] M. T. Hutchings, in *Solid State Physics*, Solid State Physics Series Vol. 16, edited by F. Seitz and D. Turnbull (Elsevier, New York, 1964), pp. 227–273.
[67] J. Banda, B. K. Rai, H. Rosner, E. Morosan, C. Geibel, and M. Brando, Phys. Rev. B **98**, 195120 (2018).
[68] G. Gruner and A. Zawadowski, Rep. Prog. Phys. **37**, 1497 (1974).
[69] N. Tsujii, J. He, K. Yoshimura, K. Kosuge, H. Michor, K. Kreiner, and G. Hilscher, Phys. Rev. B **55**, 1032 (1997).
[70] N. Tsujii, J. He, F. Amita, K. Yoshimura, K. Kosuge, H. Michor, G. Hilscher, and T. Goto, Phys. Rev. B **56**, 8103 (1997).
[71] A. Yatskar, N. K. Budraa, W. P. Beyermann, P. C. Canfield, and S. L. Bud'ko, Phys. Rev. B **54**, R3772 (1996).
[72] Z. Fisk and M. B. Maple, J. Alloys Compd. **183**, 303 (1992).
[73] M. S. Torikachvili, S. Jia, E. D. Mun, S. T. Hannahs, R. C. Black, W. K. Neils, D. Martien, S. L. Bud'ko, and P. C. Canfield, Proc. Natl. Acad. Sci. USA **104**, 9960 (2007).
[74] K. Kadowaki and S. B. Woods, Solid State Commun. **58**, 507 (1986).
[75] P. Gegenwart, T. Westerkamp, C. Krellner, M. Brando, Y. Tokiwa, C. Geibel, and F. Steglich, Phys. B (Amsterdam) **403**, 1184 (2008).
[76] J. Custers, P. Gegenwart, H. Wilhelm, K. Neumaier, Y. Tokiwa, O. Trovarelli, C. Geibel, F. Steglich, C. Pépin, and P. Coleman, Nature (London) **424**, 524 (2003).
[77] P. W. Anderson, B. I. Halperin, and C. M. Varma, Philos. Mag. **25**, 1 (1972).
[78] Y. Akagi and Y. Motome, J. Phys. Soc. Jpn. **79**, 083711 (2010).
[79] S. A. M. Mentink, A. Drost, G. J. Nieuwenhuys, E. Frikkee, A. A. Menovsky, and J. A. Mydosh, Phys. Rev. Lett. **73**, 1031 (1994).
[80] Z. Wang and C. D. Batista, arXiv:2111.13976.
[81] H. W. S. Arachchige, W. R. Meier, M. Marshall, T. Matsuoka, R. Xue, M. A. McGuire, R. P. Hermann, H. Cao, and D. Mandrus, Phys. Rev. Lett. **129**, 216402 (2022).